

# Selection of a staggered grid for inertia-gravity waves in shallow water

J. M. Beckers<sup>\*,†</sup>

*University of Liège, Sart-Tilman B5, B-4000 Liège, Belgium*

## SUMMARY

The problem of accuracy in propagating inertia-gravity waves on Arakawa grids is investigated. It is shown that the sole analysis of spatial discretization and the recommendation of the B-grid for coarse resolution models and C-grid for high resolution models must be re-analysed when time discretization is taken into account as well. For a chosen time discretization, a coarse C-grid is shown for example, to increase precision when using larger time-steps (up to the stability limit) whereas the precision of the B-grid decreases. Here, an analysis of error for different grids in function of the space–time resolutions and computational costs is presented and some recommendations on the choice of the particular staggered grid for a given application are outlined. Copyright © 2002 John Wiley & Sons, Ltd.

KEY WORDS: numerical stability; inertia-gravity waves

## 1. INTRODUCTION

Inertia-gravity waves (e.g. Reference [1]) occur and participate in numerous processes: large-scale atmospheric and oceanic motions reach geostrophic equilibrium balance by means of transient inertia-gravity waves and the dynamics of tides and storm surges are dominated by the propagation of external inertia-gravity waves, which are related to the evolution of the sea surface. In strongly stratified seas, the displacement of density surfaces also leads to (internal) inertia-gravity waves. Analytical studies (e.g. References [2–7]) of these processes are now classical parts of textbooks on geophysical fluid dynamics because of their importance.

Numerical treatment of these waves was however simplified in the past, due to limited computing power. In small domains Coriolis effects were generally neglected, whereas large-scale models neglected gravity waves.

Since the propagation of inertia-gravity waves is now also taken into account in modern numerical models, it is of paramount importance that the numerical scheme utilized to simulate

---

\*Correspondence to: J. M. Beckers, Chercheur Qualifié FNRS, University of Liège, Sart-Tilman B5, B-4000 Liège, Belgium.

†E-mail: jm.beckers@ulg.ac.be

*Received November 2000*

*Revised 28 May 2001*

these waves, which are governed by the following equations, behaves properly:

$$\frac{\partial u}{\partial t} = fv - g \frac{\partial \eta}{\partial x} \quad (1)$$

$$\frac{\partial v}{\partial t} = -fu - g \frac{\partial \eta}{\partial y} \quad (2)$$

$$\frac{\partial \eta}{\partial t} + h \left( \frac{\partial u}{\partial x} + \frac{\partial v}{\partial y} \right) = 0 \quad (3)$$

$t$  is the time;  $u$  and  $v$  are the horizontal velocity components in Cartesian  $x$  and  $y$  directions, respectively and  $\eta$  is the sea surface elevation.  $g$  is gravitational acceleration,  $f$  the constant Coriolis frequency and  $h$  is the unperturbed sea depth, which we assume to be constant here. The governing equations are generic equations, which can also be used to describe the internal inertia-gravity waves, provided that one interprets  $\eta$ ,  $u$ ,  $v$  and  $h$  as equivalent quantities related to the particular internal mode considered (e.g. Reference [8]).

Various discretized forms of Equations (1)–(3) have been examined [6, 9–13]. Generally, such studies focus on space differencing aspects by arguing that the time step can be reduced as much as need with a linear increase in cost, compared to a quadratic increase in cost for an increase in spatial resolution. Furthermore, when time differencing is also considered, it is customary to restrict the study to pure gravity waves ( $f=0$ ) for the numerical stability analysis. In this case, stability conditions and propagation properties of the numerical scheme are readily obtained, but do not take into account geostrophic adjustments. Therefore it is assumed here that the Coriolis parameter is different from zero.

In the present work the focus will be on the problem of wave propagation in a fully discretized situation as found in existing models [14], to verify, among other things, the general statement that B-grids behave better at low resolutions and that C-grids behave better at higher resolutions [15–18].

Only a two-level temporal discretization will be analysed and presented in Section 2 and for which the numerical dispersion relationship is established. Errors in propagation properties are then analysed in Section 3.

## 2. NUMERICAL SCHEME

As already shown by semi-discrete studies [12, 19], numerical propagation of Poincaré and Kelvin waves strongly depends on the distribution of  $u$ ,  $v$  and  $\eta$  over grid points. Here, only the four most widely mentioned numerical lattices are cited, namely the A, B, C and D grids, according to Arakawa's classification [10] (Figures 1–4). Using the following standard notations

$$a_{n_t, n_x, n_y} = a(t, x, y) = a(n_t \Delta t, n_x \Delta x, n_y \Delta y) \quad (4)$$

$$(\delta_x a)_{n_t, n_x, n_y} = \frac{a_{n_t, n_x+1/2, n_y} - a_{n_t, n_x-1/2, n_y}}{\Delta x} \quad (5)$$

$$(\bar{a}^x)_{n_t, n_x, n_y} = \frac{a_{n_t, n_x+1/2, n_y} + a_{n_t, n_x-1/2, n_y}}{2} \quad (6)$$

the one-time step method schemes read for the different grids:

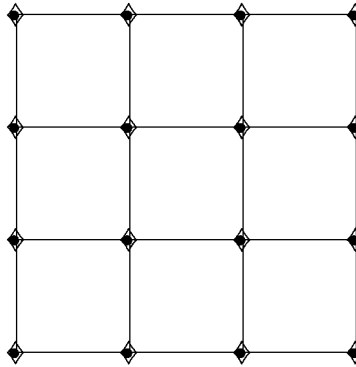


Figure 1. Arakawa A-Grid with positions of  $\eta$  points ( $\bullet$ ) and  $u$  and  $v$  points ( $\diamond$ ) at the same location.

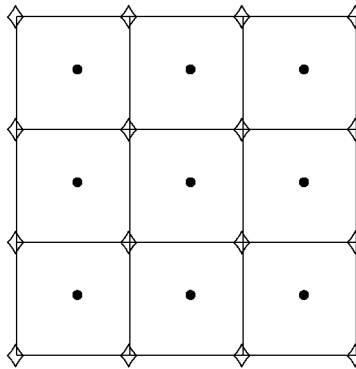


Figure 2. Arakawa B-Grid with positions of  $\eta$  points ( $\bullet$ ) in the centre of the grid box and  $u$  and  $v$  points ( $\diamond$ ) at the corners.

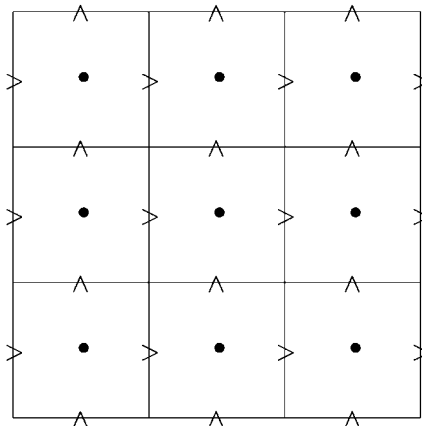


Figure 3. Arakawa C-Grid with positions of  $\eta$  points ( $\bullet$ ) in the centre of the grid box and  $u$  ( $>$ ) and  $v$  points ( $\wedge$ ) at the interfaces.

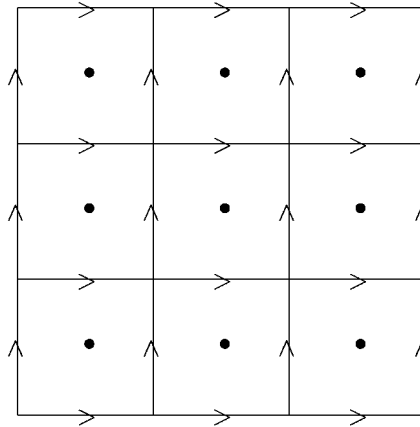


Figure 4. Arakawa D-Grid with positions of  $\eta$  points ( $\bullet$ ) in the centre of the grid box and  $u$  ( $>$ ) and  $v$  points ( $\wedge$ ) at the interfaces.

A-grid

$$(\delta_t \eta)_{n_t+1/2, n_x, n_y} + h[(\delta_x \bar{u}^x)_{n_t, n_x, n_y} + (\delta_y \bar{v}^y)_{n_t, n_x, n_y}] = 0 \quad (7)$$

$$(\delta_t u)_{n_t+1/2, n_x, n_y} - f v_{n_t+s, n_x, n_y} = -g(\delta_x \bar{\eta}^x)_{n_t+1, n_x, n_y} \quad (8)$$

$$(\delta_t v)_{n_t+1/2, n_x, n_y} + f u_{n_t+1-s, n_x, n_y} = -g(\delta_y \bar{\eta}^y)_{n_t+1, n_x, n_y} \quad (9)$$

B-grid

$$(\delta_t \eta)_{n_t+1/2, n_x, n_y} + h[(\delta_x \bar{u}^y)_{n_t, n_x, n_y} + (\delta_y \bar{v}^x)_{n_t, n_x, n_y}] = 0 \quad (10)$$

$$(\delta_t u)_{n_t+1/2, n_x+1/2, n_y+1/2} - f v_{n_t+s, n_x+1/2, n_y+1/2} = -g(\delta_x \bar{\eta}^y)_{n_t+1, n_x+1/2, n_y+1/2} \quad (11)$$

$$(\delta_t v)_{n_t+1/2, n_x+1/2, n_y+1/2} + f u_{n_t+1-s, n_x+1/2, n_y+1/2} = -g(\delta_y \bar{\eta}^x)_{n_t+1, n_x+1/2, n_y+1/2} \quad (12)$$

C-grid

$$(\delta_t \eta)_{n_t+1/2, n_x, n_y} + h[(\delta_x u)_{n_t, n_x, n_y} + (\delta_y v)_{n_t, n_x, n_y}] = 0 \quad (13)$$

$$(\delta_t u)_{n_t+1/2, n_x+1/2, n_y} - f \bar{v}_{n_t+s, n_x+1/2, n_y}^{xy} = -g(\delta_x \eta)_{n_t+1, n_x+1/2, n_y} \quad (14)$$

$$(\delta_t v)_{n_t+1/2, n_x, n_y+1/2} + f \bar{u}_{n_t+1-s, n_x, n_y+1/2}^{xy} = -g(\delta_y \eta)_{n_t+1, n_x, n_y+1/2} \quad (15)$$

D-grid

$$(\delta_t \eta)_{n_t+1/2, n_x, n_y} + h[(\delta_x \bar{u}^{xy})_{n_t, n_x, n_y} + (\delta_y \bar{v}^{xy})_{n_t, n_x, n_y}] = 0 \quad (16)$$

$$(\delta_t u)_{n_t+1/2, n_x, n_y+1/2} - f \bar{v}_{n_t+s, n_x, n_y+1/2}^{xy} = -g(\delta_x \bar{\eta}^{xy})_{n_t+1, n_x, n_y+1/2} \quad (17)$$

$$(\delta_t v)_{n_t+1/2, n_x+1/2, n_y} + f \bar{u}_{n_t+1-s, n_x+1/2, n_y}^{xy} = -g(\delta_y \bar{\eta}^{xy})_{n_t+1, n_x+1/2, n_y} \quad (18)$$

(For symmetry reasons, the switch  $s$  is zero for odd values of  $n_t$  and one for even values).

Discretization thus uses the FBTCs (Forward Backward in Time, Centered in Space) technique so as to have an efficient algorithm with as much implicit treatment as possible, without having the need to solve linear systems. Centred space differencing is the same as in Reference [10], whereas time stepping of the gravity wave part is similar to the forward-backward scheme [20]. Coriolis terms are treated by an approach [21] which uses the ‘new velocity’ only in one of the two velocity equations, so that one velocity component is computed before the second one, which in turn uses the newly computed velocity value of the other component. Another Coriolis discretization and stability conditions for a damped system may be found in Reference [22].

The von Neumann stability analysis is now applied to the discretized equations by defining a spatially periodic solution

$$(\eta, u, v) = (\mathcal{E}(t), \mathcal{U}(t), \mathcal{V}(t))e^{i(k_x x + k_y y)} = \mathbf{x}_{n_t} e^{i(n_x 2\theta_x + n_y 2\theta_y)} \tag{19}$$

where  $\theta_x$  and  $\theta_y$  are linked to the wave numbers  $k_x$  and  $k_y$  by  $0 \leq 2\theta_x = k_x \Delta x \leq \pi$  and  $0 \leq 2\theta_y = k_y \Delta y \leq \pi$  and  $i^2 = -1$ . The periodic solution (19) is then introduced into the system of discretized equations; for all grids this leads to the expression

$$\mathbf{A}_s \mathbf{x}_{n_t+1} + \mathbf{B}_s \mathbf{x}_{n_t} = 0, \quad s = 0, 1 \tag{20}$$

from which one can compute the classical amplification matrix  $\mathbf{H}_{10} = \mathbf{A}_1^{-1} \mathbf{B}_1 \mathbf{A}_0^{-1} \mathbf{B}_0$  and its characteristic equation\*  $\det(\mathbf{H}_{10} - \rho \mathbf{I}) = 0$ . Discretization constants appear in the following combinations:

$$\Phi = f \Delta t \tag{21}$$

$$(c_x^2, c_y^2) = gh \left( \frac{\Delta t^2}{\Delta x^2}, \frac{\Delta t^2}{\Delta y^2} \right) = R^2 \Phi^2 \left( \frac{\Delta t^2}{\Delta x^2}, \frac{\Delta t^2}{\Delta y^2} \right) \tag{22}$$

where we introduced the Rossby radius of deformation  $R = \sqrt{gh} f^{-1}$ . In order to study the effect of spatial resolution, it is useful to define a parameter  $r$  which measures spatial grid size compared to the Rossby radius of deformation:

$$r = \frac{R}{\sqrt{\Delta x \Delta y}} \tag{23}$$

so that

$$(c_x^2, c_y^2) = r^2 \Phi^2 \left( \gamma, \frac{1}{\gamma} \right) \tag{24}$$

where the parameter  $\gamma = \Delta y \Delta x^{-1}$  is a measure of anisotropy of the horizontal grid.

The characteristic equation reads [6]

$$(\rho - 1)(\rho^2 - 2b\rho + 1) = 0 \tag{25}$$

---

\*The same characteristic equation is obtained for the other possible definition of the amplification matrix  $\mathbf{H}_{01} = \mathbf{A}_0^{-1} \mathbf{B}_0 \mathbf{A}_1^{-1} \mathbf{B}_1$ .

Table I. Definition of parameters involved in the stability analysis and dispersion relation for A, B, C and D grids.

Grid	$\xi_*$	$\alpha$	$\xi_x/c_x^2$	$\xi_y/c_y^2$
A	4	1	$\sin^2 2\theta_x$	$\sin^2 2\theta_y$
B	1	1	$\sin^2 \theta_x \cos^2 \theta_y$	$\sin^2 \theta_y \cos^2 \theta_x$
C	1	$ \cos \theta_x \cos \theta_y $	$\sin^2 \theta_x$	$\sin^2 \theta_y$
D	1	$ \cos \theta_x \cos \theta_y $	$\alpha^2 \sin^2 \theta_x$	$\alpha^2 \sin^2 \theta_y$

where

$$b \equiv 1 - 8 \frac{(\xi_* - \xi)\xi}{\xi_*^2} - 2\Phi^2\alpha^2 \left[ 4 \frac{\xi_x \xi_y}{\xi_*^2} + \frac{(\xi_* - 2\xi)}{\xi_*} \right] \tag{26}$$

$$\xi = \xi_x + \xi_y \tag{27}$$

The different cases of A, B, C and D grids are given in Table I. From there, the stability condition  $|b| \leq 1$  can be translated into conditions on the discretization constants  $\Phi, c_x, c_y$ .

Furthermore, the amplification factor  $\rho$  allows comparing the numerical propagation to the physical dispersion relation, which is

$$\left(\frac{\omega}{f}\right)^2 = 1 + (k_x^2 + k_y^2)R^2 = 1 + 4(\theta_x^2 + \theta_y^2)r^2 \tag{28}$$

whereas the numerical dispersion relationship reads

$$\omega^N = \frac{\arg \rho}{2\Delta t} \tag{29}$$

The factor  $2\Delta t$  stems from the fact that a full cycle of temporal discretization consists in two successive time-steps ( $n_t$  even and  $n_t$  odd) to take into account alternating treatments of the Coriolis term. Since  $\rho = b \pm i\sqrt{1 - b^2}$ ,  $\omega^N$  is readily calculated and allows assessing the numerical propagation properties of the schemes:

$$\left(\frac{\omega^N}{f}\right)^2 = \frac{\theta^2}{4\Phi^2}, \quad \cos \theta = b \tag{30}$$

For small time-steps ( $\Phi \rightarrow 0$ ,  $r$  fixed),

$$b \sim 1 - \frac{8r^2\Phi^2}{\xi_*} (\gamma \xi_x c_x^{-2} + \gamma^{-1} \xi_y c_y^{-2}) - 2\Phi^2\alpha^2 \tag{31}$$

so that

$$\left(\frac{\omega^N}{f}\right)^2 = \frac{1}{4\Phi^2} (\arccos b)^2 \sim \frac{1}{4\Phi^2} 2(1 - b) \sim \frac{4r^2}{\xi_*} (\gamma \xi_x c_x^{-2} + \gamma^{-1} \xi_y c_y^{-2}) + \alpha^2 \tag{32}$$

Table II. Stability limits of A, B, C and D grids.

Grid	$c_{\text{lim}}^2$
A	$2 \frac{(2 -  \Phi  - \Phi^2)}{4 - \Phi^2}$
B	$\frac{(1 - \Phi^2)}{2}$
C	$\frac{1}{4}$
D	$\min_{z \in [0,1]} \left[ \frac{(1 - z \Phi )}{2z^2(1-z)(2-z \Phi )} \right]$

By using the definitions of Table I, one retrieves the classical dispersion relationship of the semi-discrete case [12].<sup>†</sup> If in addition  $\Delta x \rightarrow 0$ ,  $\Delta y \rightarrow 0$ , this can be further developed in terms of small  $\theta_x$ ,  $\theta_y$ , and in this case one retrieves the physical dispersion relationship (28), indicating that a consistent discretization has been used.

The numerical propagation properties of the fully discretized scheme can now be compared to the physical continuous wave propagation.

### 3. NUMERICAL PROPAGATION PROPERTIES

In the following, the study will be limited to the case where  $\gamma = 1$ . On the one hand, assuming an anisotropic grid leads to cumbersome stability criteria [23] and on the other hand, for an analysis of the wave propagation error (which we would like to keep as low as possible), it would seem strange to allow strongly anisotropic grids. In any case, most studies of spatial discretization error already restrict the analysis to this case. Therefore an analysis of the additional effects of temporal discretizations will be coherent with previous studies. Should one want to calculate errors in the case of an anisotropic or 1D grid, the previous general calculations remain valid and could be used to assess the effect of anisotropy.

In the isotropic case,  $c_x = c_y = c$ , and the necessary and sufficient stability conditions read

$$\Phi^2 \leq 1 \quad (33)$$

$$c^2 \leq c_{\text{lim}}^2 \quad (34)$$

where  $c_{\text{lim}}$  is given in Table II for each grid. To characterize error in the propagation, one generally analyses the relative error  $\varepsilon$  defined by

$$\varepsilon = \frac{\omega^N - \omega}{\omega} \quad (35)$$

<sup>†</sup>By observing that  $1 - \cos 2\theta_x \cos 2\theta_y = 2(\sin^2 \theta_x \cos^2 \theta_y + \sin^2 \theta_y \cos^2 \theta_x)$ .

and an average error  $\bar{\varepsilon}$

$$\bar{\varepsilon}^2 \equiv \frac{1}{\theta_*^2} \int_0^{\theta_*} \int_0^{\theta_*} \varepsilon^2 d\theta_x d\theta_y \quad (36)$$

Since grid noise is usually filtered out and because errors are only analysed for smaller wave numbers, authors generally disregard waves whose wave number is higher than  $\theta_* = \pi/4$ .

Another property is group velocity  $\mathbf{C} = C_x \mathbf{e}_x + C_y \mathbf{e}_y$ :

$$C_x = \frac{\partial \omega}{\partial k_x} = \frac{\Delta x}{2} \frac{\partial \omega}{\partial \theta_x}, \quad C_y = \frac{\partial \omega}{\partial k_y} = \frac{\Delta y}{2} \frac{\partial \omega}{\partial \theta_y} \quad (37)$$

and its numerical counterpart  $\mathbf{C}^N = C_x^N \mathbf{e}_x + C_y^N \mathbf{e}_y$

$$C_x^N = \frac{\partial \omega^N}{\partial k_x} = \frac{\Delta x}{2} \frac{f}{2\Phi} \frac{\partial \theta}{\partial \theta_x}, \quad C_y^N = \frac{\partial \omega^N}{\partial k_y} = \frac{\Delta y}{2} \frac{f}{2\Phi} \frac{\partial \theta}{\partial \theta_y} \quad (38)$$

With these, we can calculate an error norm for group velocity:

$$\varepsilon_g = \frac{\|\mathbf{C}^N\| - \|\mathbf{C}\|}{\|\mathbf{C}\|} \quad (39)$$

For extremely small time-steps, we recover the known results and conclusions for the choice of the B or C-grid depending on whether the radius of deformation is well resolved ( $r > 1$ ) or not. Indeed, Figure 5 at the marginal resolution  $r = 1$  in function of the wavelength shows a similar average error for B and C-grids and higher errors for the A and D-grids. Figure 6 shows the corresponding error on group velocity. For medium resolution, classical results are retrieved, showing for very small time-steps the more uniform behaviour of the C-grid for all wavelengths and large errors for higher wave numbers in the other grids. Figure 7 is typical for results used to justify the recommendation of the B-grid for coarse resolutions, since as shown, for small values of  $r$ , the errors for a specific wave ( $\theta_x = \theta_y$ ) are lower than for the C-grid for all well resolved wavelength.

One can now verify if this conclusion holds for larger time-steps.

For medium size time-steps ( $\Phi = 0.3$ ), the phase speed error (Figure 8) for the medium resolution indicates a slight increase in errors for the B-grid and a decrease for the C-grid. This also holds for group velocity (not shown). In order to quantify the errors in terms of spatial and temporal resolution, average errors (averages on the wavelength of Equation (36)) are now used and contoured in the  $(r, \phi)$  space. This is done in Figure 9, and it is readily seen that A and B-grids actually increase their average errors for higher resolutions, whereas the C-grid decreases its error for higher resolutions. In order to have a better quantitative comparison, a look at Figures 10 and 11 shows the average errors for the different grids in function of the temporal resolution for different spatial resolutions. It is readily seen that indeed, for smaller time-steps, the B-grid has an advantage over the C-grid and that the D-grid performs poorly (as expected). On the other hand, one can clearly observe that the C-grid increases its precision for increased time-steps at lower resolutions, whereas the B-grid error increases, so that there exists a time-step at which both grids have an identical average error. For larger time steps the C-grid performs even better. When higher resolutions are considered,

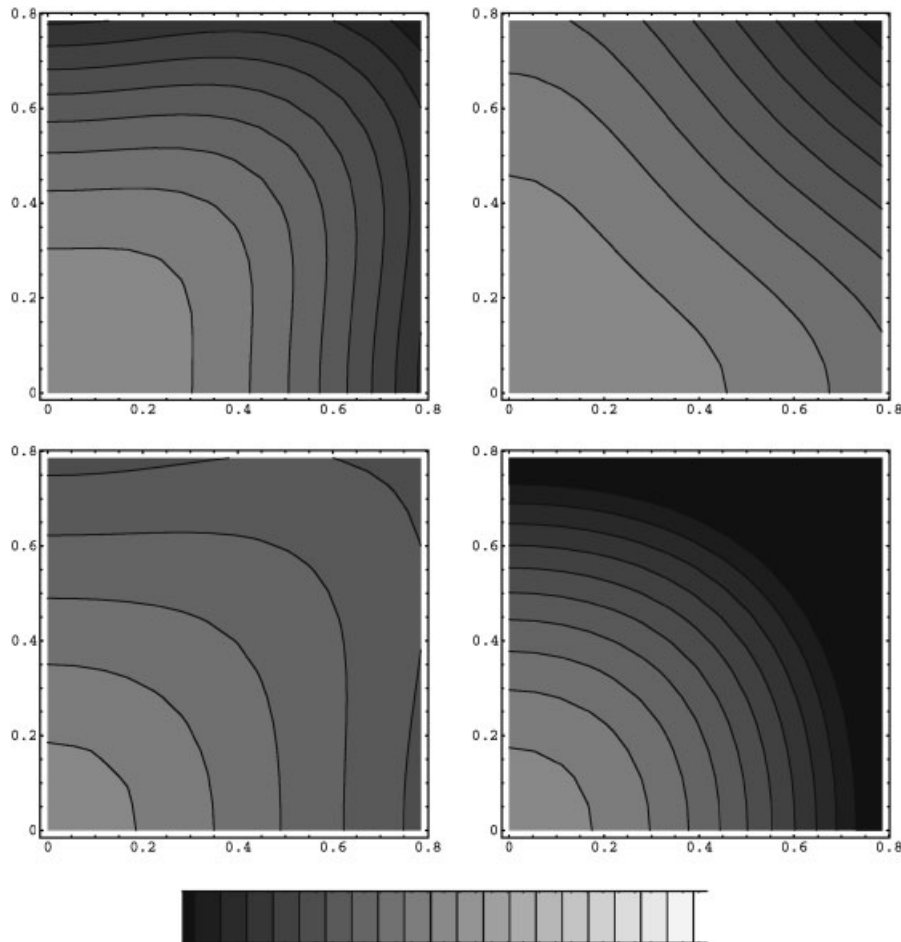


Figure 5. Relative error  $\varepsilon$  ( $r=1, \Phi=10^{-4}$ ) for A grid (upper left panel), B grid (upper right panel), C grid (lower left panel) and D grid (lower right panel), in function of  $\theta_x, \theta_y$ . Grey level scales indicate values from  $-0.33$  (black) to  $0.33$  (white).

the effect of changing the time-step is less marked and similar for all grids, so that a grid which performs better at a higher spatial resolution maintains its advantage when changing the time-step (up to the stability limit). Therefore, one could conclude that the C-grid could reach the same precision as the B-grid when the time-step is increased towards the stability limit, something one is tempted to do in most models in order to reduce computational costs. However, instead of decreasing the time-resolution to decrease computational costs, one could also decide to reduce the spatial resolution and to keep a finer time-step (especially for the B-grid of course).

Therefore, when comparing schemes and possible choices of resolutions in both spatial and temporal domains, the concept of computational cost should be included in the discussion. To do so, one can consider that a system with a fixed spatial domain and a given time interval

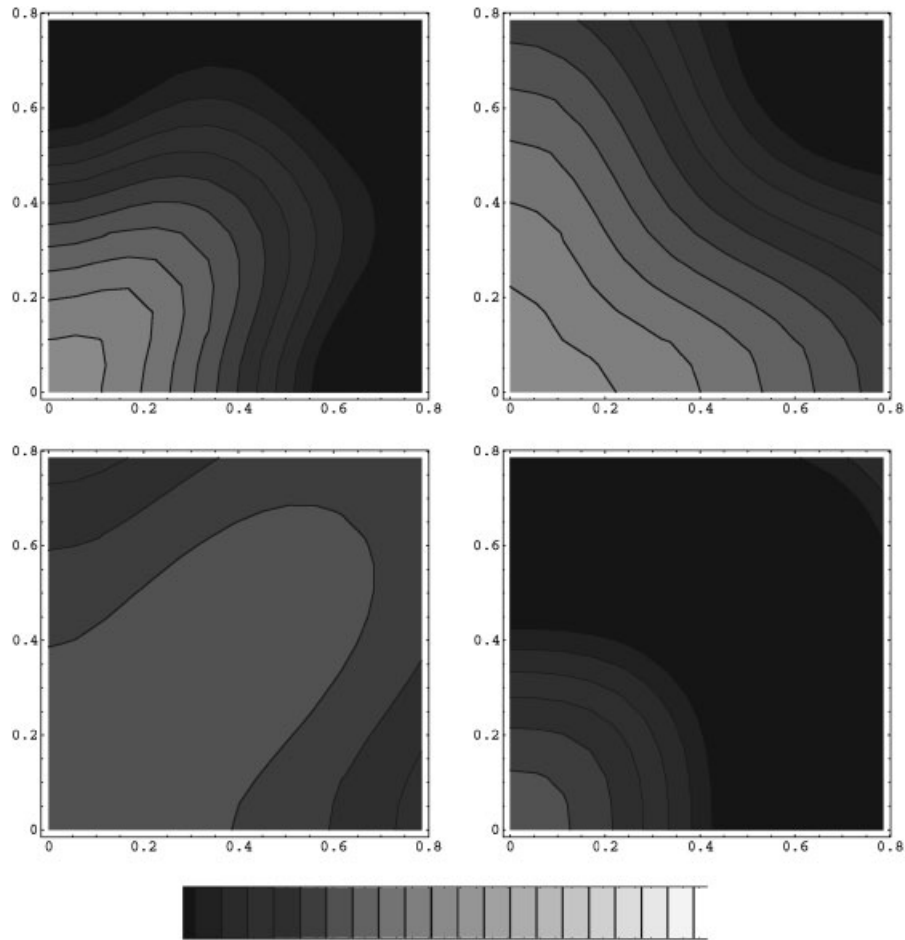


Figure 6. Relative error  $\varepsilon_G$  of group velocity ( $r=1, \Phi=10^{-4}$ ) for A grid (upper left panel), B grid (upper right panel), C grid (lower left panel) and D grid (lower right panel), in function of  $\theta_x, \theta_y$ . Grey level scales indicate values from  $-0.66$  (black) to  $0.66$  (white).

is simulated, in which case the total number of operations  $N$  is given by

$$N = \beta r^2 / \Phi \quad (40)$$

where  $\beta$  is a constant parameter depending on the size of the domain and the simulated real time. This means that a curve of constant cost is given by

$$\log(\Phi) = 2 \log(r) + C \quad (41)$$

For large values of  $C$ , the scheme is on the low resolution and economic side, whereas for small values of  $C$  a high resolution and costly discretization is chosen.

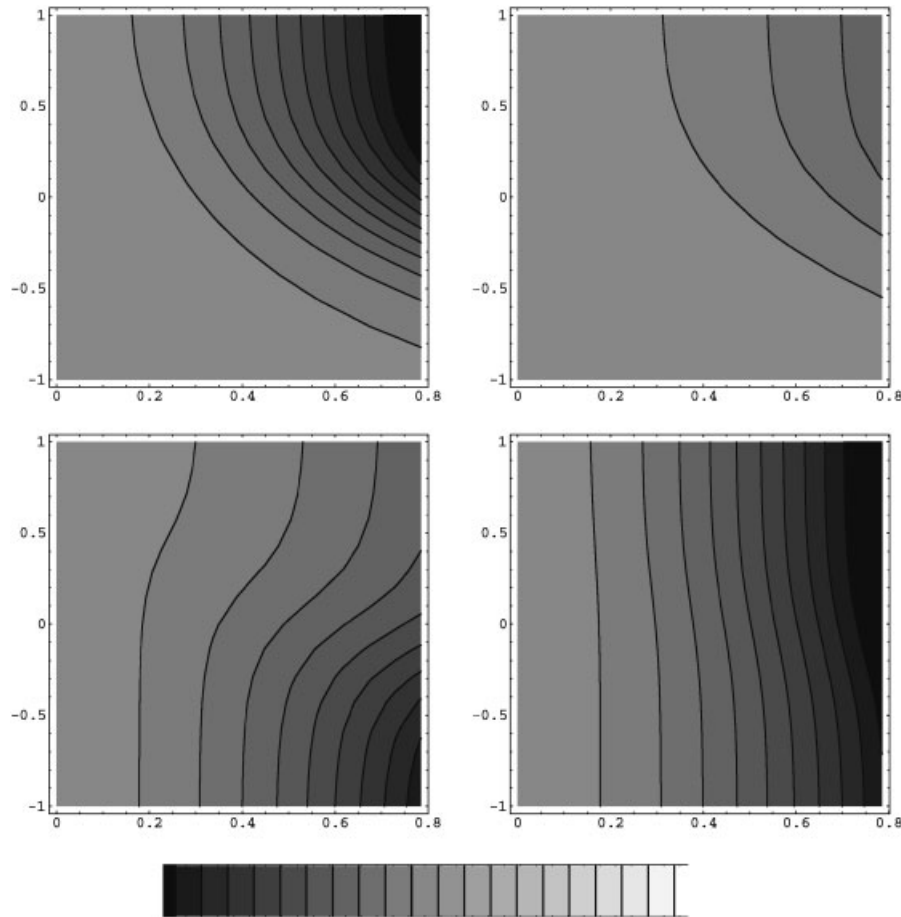


Figure 7. Relative error  $\varepsilon$ , ( $\Phi=10^{-4}$ ) for A grid (upper left panel), B grid (upper right panel), C grid (lower left panel) and D grid (lower right panel), in function of  $\theta_x$  and  $\log(r)$  ( $\theta_y=\theta_x$ ). Grey level scales indicate values from  $-0.33$  (black) to  $0.33$  (white).

When comparing schemes for constant cost, one must bear in mind that if spatial resolution is increased, smaller wavelengths are resolved. These waves should however not be taken into account for the comparison, since the question to be solved is the following: assuming that one wants to resolve wavelength down to  $\lambda=R\delta$ , where  $\delta$  is a fixed parameter, and that one will keep the computational cost constant, should one use an increased resolution in space or in time? Then the criteria of choice is the average error of the propagation scheme for waves with wavelengths larger than  $\lambda$ , even if the grid chosen allows to resolve finer scales.

Definitively, once one has decided that the smallest wavelength of interest is  $\lambda$ , one should have a spatial resolution which at least corresponds to  $\theta_*=\pi/4=\pi\Delta x\lambda^{-1}$  if one does, as usual, consider that the numerical grid does not correctly represent small scale waves above  $k_x\Delta x=\pi/2$ . This means that one should have  $r\delta\geq 4$ . For computation of the average error, one must then limit the integration of Equation (36) corresponding to the wavelength  $\lambda$ , which

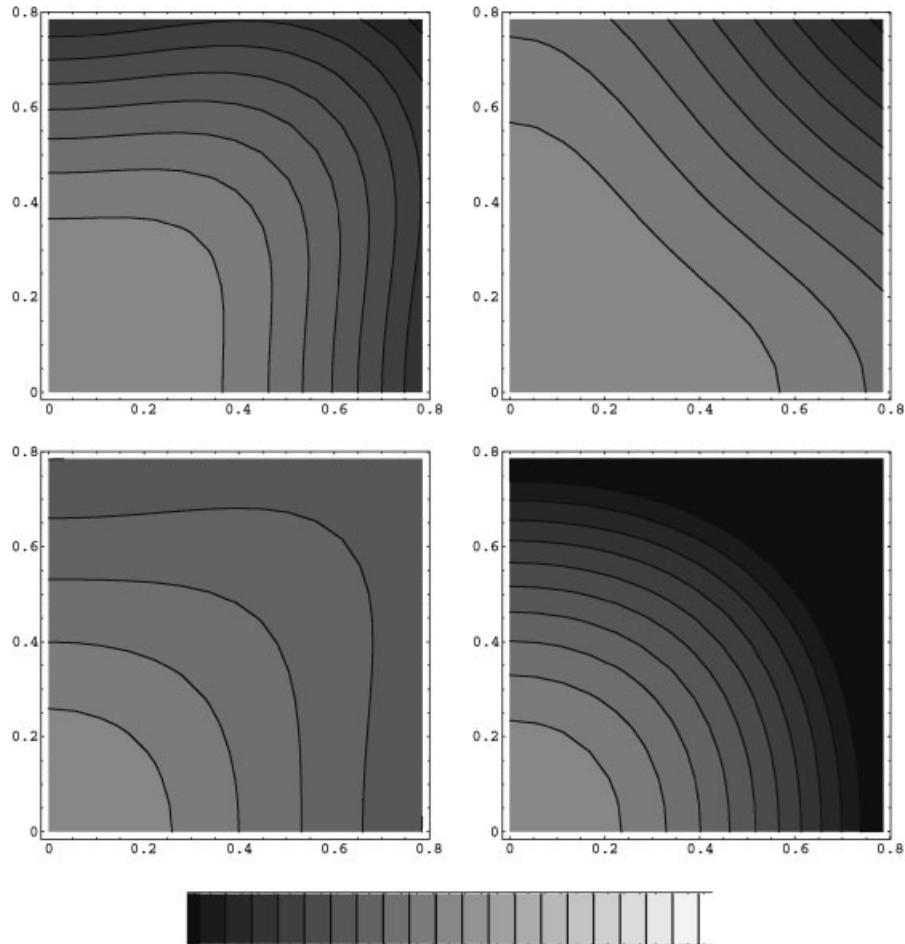


Figure 8. Relative error  $\varepsilon$  ( $r=1, \Phi=0.3$ ) for A grid (upper left panel), B grid (upper right panel), C grid (lower left panel) and D grid (lower right panel), in function of  $\theta_x, \theta_y$ . Grey level scales indicate values from  $-0.33$  (black) to  $0.33$  (white).

gives

$$\theta_* = \frac{\pi}{4} \frac{4}{r\delta} \quad (42)$$

One can then compare schemes which resolve well the radius of deformation ( $\delta \ll 1$ ), marginally resolve it ( $\delta \sim 1$ ), or do not resolve it ( $\delta \gg 1$ ). Concerning computational cost, if one wants to be able to use larger time steps when increasing spatial resolution, to keep computational cost constant, we must take

$$\log(\Phi) = 2 \log(r) + \log(\Phi_0) - 2 \log(r_0) \quad (43)$$

where  $\Phi_0$  and  $r_0$  are such that the lowest possible spatial resolution  $r_0 = 4\delta^{-1}$  has a time-stepping that is well below the stability limit (otherwise there would be no possibility of

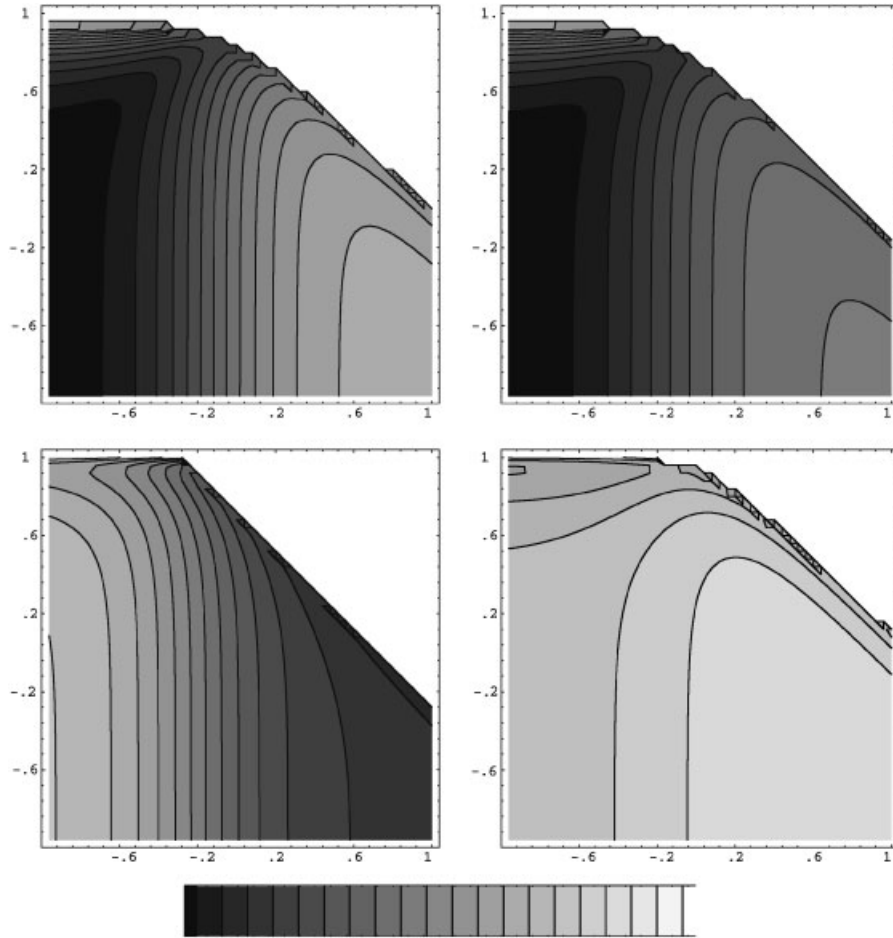


Figure 9. Average  $\bar{\epsilon}$ , for A grid (upper left panel), B grid (upper right panel), C grid (lower left panel) and D grid (lower right panel), in function of  $\log(r)$  and  $(1 + \log(\Phi))$ . Grey level scales indicate values from 0 (black) to 0.3 (white).

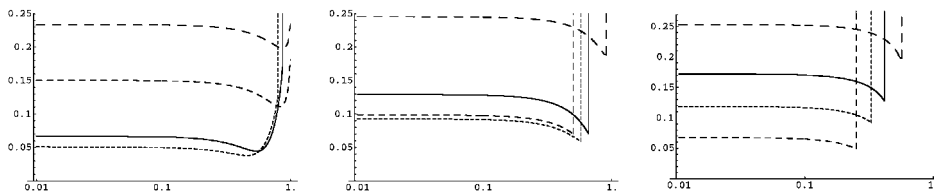


Figure 10. Average error  $\bar{\epsilon}$ , for A grid (continuous line), B grid (fine grain dashed line), C grid (medium grain dashed line) and D grid (coarse grain dashed line), in function of  $1 + \log(\Phi)$ . Coarser resolution  $r = 0.5$  (left), medium resolution  $r = 1$  (middle) and higher resolution  $r = 2$  (right).

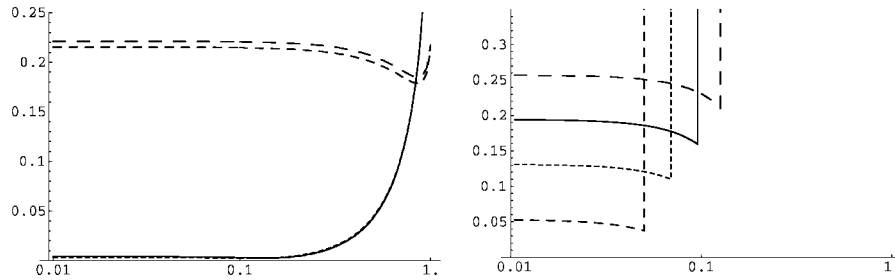


Figure 11. Average error  $\bar{\epsilon}$ , for A grid (continuous line), B grid (fine grain dashed line), C grid (medium grain dashed line) and D grid (coarse grain dashed line), in function of  $1 + \log(\Phi)$ . Very coarse resolution  $r=0.1$  (left), and very high resolution  $r=10$  (right).

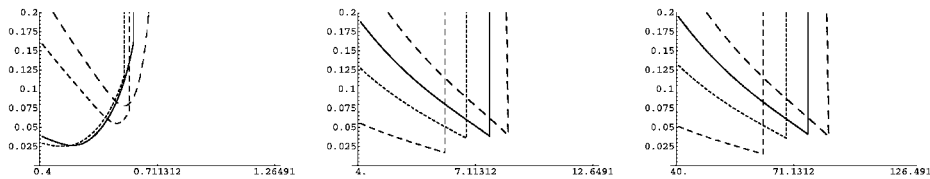


Figure 12. Average  $\bar{\epsilon}$ , for A grid (full line), B grid (fine dash line), C grid (medium dashed line) and D grid (large dashed lines), in function of  $\log(r)$  for constant cost.  $\delta=10$  (left),  $\delta=1$  (middle) and  $\delta=0.1$  (right).

increasing spatial resolution at constant cost). Here,

$$\Phi_0^2 = \frac{\mu}{\mu + r_0^2} \quad (44)$$

was chosen, with  $\mu=0.02$ , which corresponds to  $c^2 = \mu(1 - \Phi^2)$ .

By comparing the grids used in cases for unresolved radius, marginally resolved and well resolved (Figure 12), one observes that at constant cost, the C-grid can be made almost as precise as the B-grid, even for large-scale models, but with an increased spatial resolution compared to the B-grid. In this case the time-stepping of the B-grid is finer. For the other cases, the C-grid always performs better than the B-grid.

#### 4. SEMI-IMPLICIT SCHEMES

Since it was shown that on the C-grid, a larger time-step can actually decrease propagation error, it might be interesting to investigate implicit or semi-implicit schemes, since they are not limited by a stability condition. Then maybe an even increased time step (at an increased cost for solving a linear system) could reduce the error even more or maintain it at an acceptable level.

To analyse this possibility, only the C-grid is investigated, as it is the most promising candidate. When turning towards an implicit scheme, one loses the advantage of the previous scheme that does not need to solve any linear system, since the algorithmic calculations

are explicit. When using the semi-implicit or implicit scheme, one could then also treat the Coriolis term with a classical implicit discretization, rather than with the Siliecki approach used up to now.

For comparison with the previous analysis, both approaches will be investigated. Then remains the choice of a fully implicit, semi-implicit or any other weighting.

The only implicit scheme on gravity wave components that does not damp waves is the trapezoidal (or semi-implicit) scheme. The fully implicit scheme damps the waves and would introduce additional errors. Here only undamped waves are considered. Should damping be necessary for some reason, an explicitly introduced diffusion would allow a better control of the damping.

If one uses a classical semi-implicit scheme on the pressure gradient and velocity divergence, amplification factors can be calculated readily.

In the case where the Coriolis discretization is done as before, one finds with the same notations as before

$$b = 1 + 2 \frac{\Phi^2 \alpha^2 (\xi - 1) - 4\xi}{(\xi + 1)^2 - \alpha^2 \Phi^2 \xi_x \xi_y} \quad (45)$$

For the full trapezoidal or fully semi-implicit scheme, also on Coriolis term,<sup>‡</sup> one finds

$$b = -1 + 2 \left( \frac{\alpha^2 \Phi^2 + 4\xi - 4}{\alpha^2 \Phi^2 + 4\xi + 4} \right)^2 \quad (46)$$

and one sees that the scheme is unconditionally stable and not damping.

Once the amplification factor is known, one can redo the error analysis and compare it with the previous explicit approach.

Figure 13 show the errors for the C-grid semi-implicit scheme with the two choices for Coriolis treatment.

Comparing with Figure 9 shows that for small time steps, errors are similar; when looking at the error in the region where the explicit scheme is unstable (upper right white triangle in contour plot of C-grid error), one can clearly see that the error for the semi-implicit scheme rapidly increases when going far beyond the CFL stability limit of the explicit scheme, a typical behaviour of semi-implicit schemes [24]. For clarity, in Figure 13, on the right part, the scale was changed by a factor 3.

Differences between the treatment of Coriolis term remain weak except near  $\Phi = 1$ , as one should expect.

Since the semi-implicit scheme is much more expensive per time-step than explicit schemes, it is only interesting to use it if one does not need an accurate propagation of the waves and can use time steps well beyond the CFL limit. Otherwise, an explicit scheme near the CFL limit behaves just as well as the implicit scheme at lower cost, but reduced robustness.

<sup>‡</sup>For the fully trapezoidal scheme, a single time-step analysis is in principle possible, but for a coherent presentation the amplification factor is still calculated over two successive time-steps.

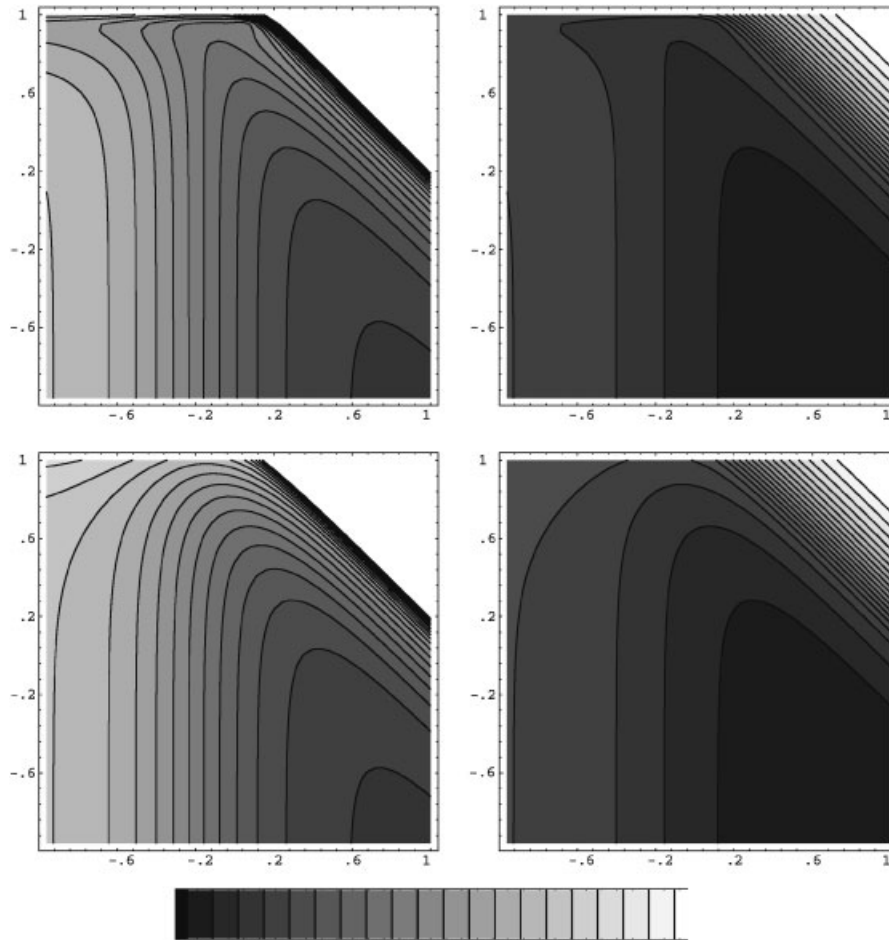


Figure 13. Average  $\bar{\epsilon}$ , for C grid with Sielecki and semi implicit scheme above (left normal scale, right  $\epsilon/3$ ). Below fully semi-implicit scheme. Error in function of  $\log(r)$  and  $(1 + \log(\Phi))$ . Grey level scales indicate values from 0 (black) to 0.3 (white).

## 5. DISCUSSION

Differences between B and C grid representations of inertia-gravity waves decrease when larger time steps are used at coarse resolutions, whereas previous authors have argued that a B grid should be used. Since most of the time, the largest possible time-step is used, the argument based on analysing the purely spatial discretization error may thus be misleading.

It was shown here that C-grid errors are always reduced when using the largest possible time-stepping, whereas B-grid errors are reduced by using small time-steps at low resolutions and larger time-steps at finer spatial resolutions.

Based on the error analysis of the present paper, the following recommendations can be made:

- (i) At low spatial resolutions and fine temporal resolutions, the B-grid would be the best choice. Any additional CPU resources should then be used to decrease the time step.
- (ii) At high spatial resolutions, the C-grid should always be preferred and be used with a time-step near the CFL limit. Additional resources should then be spent on increasing spatial resolution.
- (iii) In other cases, the C-grid should be preferred if the time-step can be chosen near the CFL limit.
- (iv) Semi-implicit schemes for the C-grid are only interesting if a very robust scheme is necessary or if one is not interested in the correct propagation of waves.

The particular results presented here certainly depend upon the specific time-discretization chosen, but even if the results cannot be immediately transposed to other time-discretizations (like the commonly used leapfrog method), or situations with rapid variations in depth  $h$ , they suggest, at least, that one should more closely look at the time-discretization effects before judging that a given spatial grid is better suited for a given situation. The fact that most of the time, the largest allowable time-step is used in real numerical simulations, reinforces the need for such an analysis, as the general argument that the time step can be reduced as desired is never met in practise.

#### ACKNOWLEDGEMENTS

A model intercomparison was supported by the European Union (MEDMEX contract MAS2-CT94-0107 and MATER contract MAS3-CT96-0051) and led to some questions addressed in the present paper. The MEDNET project (MAS3-CT96-0051) also contributed to the present paper MEDNET (MAST contract MAS3-CT98-0189) allowed to perform the analysis. Two anonymous reviewers are acknowledged for their constructive comments.

#### REFERENCES

1. Rossby C. On the mutual adjustment of pressure and velocity distributions in certain simple current systems, part 1. *Journal of Marine Research* 1937; **1**:15–28.
2. Cahn A. An investigation of the free oscillations of a simple current system. *Journal of Meteorology* 1945; **2**:113–119.
3. Obukhov AM. On the question of the geostrophic wind (in Russian). *Izvestiya Akademii nauk SSSR Seriya Geografskiya-Geofizicheskaya* 1949; **13**:281–306.
4. Washington WA. A note on the adjustment towards geostrophic equilibrium in a simple fluid system. *Tellus* 1964; **16**:530–534.
5. Blumen W. Geostrophic adjustment. *Reviews of Geophysics and Space Physics* 1972; **10**:485–528.
6. Schoenstadt AL. The effect of spatial discretization on the steady state and transient behavior of a dispersive wave equation. *Journal of Computational Physics* 1977; **23**:364–379.
7. Hsieh WW, Gill AE. The Rossby adjustment problem in rotating, stratified channel, with and without topography. *Journal of Physical Oceanography* 1984; **8**:424–437.
8. LeBlond PH, Mysak LA. *Waves in the Ocean*. Elsevier: New York, 1978; 602.
9. Schoenstadt AL, Williams RT. The computational properties of the schuman pressure gradient averaging technique. *Journal of Computational Physics* 1976; **21**:166–177.
10. Arakawa A, Lamb VR. Computational design of the basic dynamical processes of the UCLA general circulation model. Volume 17 of *Methods in Computational Physics*. Academic Press, 1977; 1–337.
11. Batteen ML, Han YJ. On the computational noise of finite-difference schemes used in ocean models. *Tellus* 1981; **33**:387–396.

12. Haidvogel D, Beckmann A. Numerical ocean circulation modeling. Volume 2 of *Series of Environmental Science and Management*. Imperial College Press, 1999; 1–318.
13. Adcroft A, Hill C, Marshall J. A new treatment of the Coriolis terms in C-grid models at both high and low resolutions. *Monthly Weather Review* 1999; **127**:1928–1936.
14. Beckers J-M. Application of a 3D model to the Western Mediterranean. *Journal of Marine Systems* 1991; **1**:315–332.
15. Song Y, Tang T. Dispersion and group velocity in numerical schemes for three-dimensional hydrodynamic equations. *Journal of Computational Physics* 1993; **105**:72–82.
16. Dukowicz J. Mesh effects for Rossby waves. *Journal of Computational Physics* 1995; **119**:188–194.
17. Wajsovicz R. Free planetary waves in finite-difference numerical models. *Journal of Physical Oceanography* 1986; **16**:773–789.
18. Randall DA. Geostrophic adjustment and the finite-difference shallow-water equations. *Monthly Weather Review* 1994; **122**.
19. Hsieh W, Davey M, Wajsovicz R. The free Kelvin wave in finite-difference numerical models. *Journal of Physical Oceanography* 1983; **13**:1383–1397.
20. Mesinger F. A method for construction of second-order accuracy difference schemes permitting no false two-grid-interval wave in the height field. *Tellus* 1973; **25**:444–458.
21. Sielecki A. An energy conserving difference scheme for the storm surge equations. *Monthly Weather Review* 1967; **96**:150–156.
22. Beckers J-M. On some stability properties of the discretization of the damped propagation of shallow-water inertia-gravity waves on the Arakawa B-grid. *Ocean Modelling* 1999; **1**:53–69.
23. Beckers J-M, Deleersnijder E. Stability of a FBTCs scheme applied to the propagation of shallow-water inertia-gravity waves on various space grids. *Journal of Computational Physics* 1993; **108**:95–104.
24. Durran D. Numerical methods for wave equations in geophysical fluid dynamics. Volume 32 of *Texts in Applied Mathematics*. Springer, 1999.